CILAMCE 2017
Florianópolis - Santa Catarina - Brazil

A Multiscale Hybrid-Mixed Method for the Elastodynamic Model with Rough Coefficients

Antônio Tadeu Azevedo Gomes

Weslley da Silva Pereira

Roberto Pinto Souto

Frédéric Valentin

atagomes@lncc.br

weslleyp@lncc.br

rpsouto@lncc.br

valentin@lncc.br

Laboratório Nacional de Computação Científica (LNCC)

Av. Getúlio Vargas, 333 - Quitandinha, 25651-075, Petrópolis, RJ, Brazil

Diego Paredes Concha

diego.paredes@pucv.cl

Pontificia Universidad Católica de Valparaíso

Av. Brasil 2950, 2340025 Valparaíso, Región de Valparaíso, Chile

Abstract. *We present a family of multiscale finite element methods for the linear elastodynamic model with highly heterogeneous coefficients, named Multiscale Hybrid-Mixed (MHM) methods. The MHM method consists of a strategy that naturally incorporates multiple scales in the numerical solutions while providing solutions with high-order precision for the primal and dual variables. It is a consequence of a hybridization procedure, which characterizes the unknowns as a direct sum of a coarse solution and the solutions to local problems with boundary conditions driven by the Lagrange multipliers. The completely independent local problems are embedded in the upscaling procedure, and computational approximations may be naturally obtained in a parallel computational environment. Numerical results verify the optimal convergence of the method, and its capacity to accurately incorporate heterogeneity and high-contrast coefficients in the numerical solution.* ***Keywords:*** *elastodynamic equations, finite element, multiscale, wave propagation*

1 INTRODUCTION

Wave propagation in heterogeneous media represents a big challenge for numerical methods in view of computational simulations. In a broad sense, very fine meshes must be adopted to approximate the high-frequency field distributions as they are greatly impacted by the multiscale structures or/and the high contrast of the medium. The idea of using high-order polynomial interpolations on coarse meshes, as proposed in Hesthaven (2003) for instance, is not a feasible option since interfaces between different material media and faces of the partition must coincide to avoid spurious numerical modes. Consequently, effective numerical methods for long-time simulations require a fine mesh to fit the complex geometry with high-order approximation to minimize dispersion.

Multiscale finite element methods have attracted great attention with their capacity to be accurate on coarse meshes (see Arbogast (2004)-Abdulle et al. (2012)-Efendiev and Wu (2002) just to cite a few). Beginning with the seminal work Babuska and Osborn (1983), the multiscale methods were further extended to higher dimensions in Hou and Wu (1997). The approach carries the concept of multiscale basis functions, which upscale to the coarse mesh. They are driven by independent local problems which turn out to be a strategy to circumvent faults and to allow spatial and time data locality while taking full advantage (in terms of performance) of the granularity of the new generation of computer architectures.

Recently, the classical hybridization procedure Raviart and Thomas (1977) has been used to devise a new family of high-order multiscale finite element method called MHM method. Particularly adapted to handle multiscale and/or high contrast coefficients on coarse meshes, the MHM method permits face-crossing interfaces endowed in local boundary conditions. Originally proposed for the Laplace problem in Harder et al. (2013), the MHM method has been analyzed in Araya et al. (2013) and extend to the elasticity and Stokes models in Harder et al. (2016) and Araya et al. (2017). It gives rise to a staggered algorithm, which first computes the multiscale basis functions from completely independent element-wise problems, and next obtains the degrees of freedom on faces from the global face-based formulation define on a coarse mesh.

This work extends the MHM method originally proposed in Harder et al. (2016) to the second order elastodynamic model with the upshot that highly heterogeneous or high-contrasted physical coefficients are allowed as found in seismic problems. It results in a *new* domain decomposition algorithm which is shown to (i) be precise on coarse meshes through upscaling, (ii) produce optimal and high-order superconvergent displacement, velocity and stress, (iii) conserve the total energy, (iv) handle high contrast interfaces on not-aligned meshes, (v) be adapted to extreme-scale parallel.

The paper is organized as follows: The next section states the problem and addresses some preliminary theoretical results. The characterization of the exact fields in terms of global-local problems is the subject of Section 3. Section 4 is devoted to the one-level and two-level MHM methods, and Section 5 is dedicated to the numerical validation of the MHM method. Conclusions follow in Section 6.

2 MODEL PROBLEM

Let $\Omega \subset \mathbb{R}^d$, $d \in \{2, 3\}$ be an open bounded domain with Lipschitz boundary $\partial\Omega = \Gamma_D \cup \Gamma_N$, where $\Gamma_D \cap \Gamma_N = \{0\}$, subjected to a distributed load $\boldsymbol{f}$ and T the final time. Under the infinitesimal strain theory, the equation of motion is given by

$$\rho \partial_{tt} \boldsymbol{u} - \nabla \cdot \boldsymbol{\sigma} = \boldsymbol{f} \quad \text{in } \Omega \times (0, T), \tag{1}$$

where ρ is the mass density, t is the time variable, $\boldsymbol{x}$ is a typical point in Ω, $\boldsymbol{u}$ is the displacement vector field and $\boldsymbol{\sigma}$ is the stress tensor. In addition to the unknowns $\boldsymbol{u}$ and $\boldsymbol{\sigma}$, we define the velocity field $\boldsymbol{v} := \partial_t \boldsymbol{u}$. For simplicity, we assume that the homogeneous Dirichlet boundary condition and the free surface condition are prescribed on Γ_D and on Γ_N, respectively. Other boundary conditions, as absorbing boundary conditions, can be imposed and easily incorporated in what follows.

We assume that the stress is linearly proportional to strain ($\boldsymbol{\varepsilon}$), i.e.,

$$\boldsymbol{\sigma} := \mathsf{C}\, \boldsymbol{\varepsilon}, \tag{2}$$

where the fourth-order stiffness tensor C acts on the space $\mathbb{R}^{d \times d}_{sym}$ of $d \times d$ symmetric matrices with values in $\mathbb{R}^{d \times d}_{sym}$. The stiffness tensor is quite general, possibly embedding multiple geometrical scales on Ω. We assume C is symmetric ($\mathsf{C}_{ijkl} = \mathsf{C}_{jikl} = \mathsf{C}_{klij}$), uniformly positive and uniformly bounded, i.e., there exist positive constants c_{min} and c_{max} such that

$$c_{min} |\boldsymbol{\varepsilon}|^2 \leqslant \mathsf{C}\, \boldsymbol{\varepsilon} : \boldsymbol{\varepsilon} \leqslant c_{max} |\boldsymbol{\varepsilon}|^2 \qquad \text{for all } \boldsymbol{\varepsilon} \in \mathbb{R}^{d \times d}_{sym}. \tag{3}$$

We denote by $\boldsymbol{u} \cdot \boldsymbol{v}$ and $\boldsymbol{\sigma} : \boldsymbol{\tau}$ the usual inner products in spaces $\mathbb{R}^d$ and $\mathbb{R}^{d \times d}$, respectively, and $|\boldsymbol{u}|$ stands for the norms induced by such inner products. Under the infinitesimal strain theory, strain is defined as the symmetric part of the gradient of $\boldsymbol{u}$, i.e.,

$$\boldsymbol{\varepsilon}(\boldsymbol{u}) := \frac{\nabla \boldsymbol{u} + (\nabla \boldsymbol{u})^T}{2}. \tag{4}$$

Collecting the previous definitions, the second-order elastodynamic problem reads: Find $\boldsymbol{u} : \Omega \times (0, T) \to \mathbb{R}$ such that

$$\begin{cases} \rho \partial_{tt} \boldsymbol{u} - \nabla \cdot \boldsymbol{\sigma}(\boldsymbol{u}) = \boldsymbol{f} & \text{in } \Omega \times (0, T], \\ \boldsymbol{\sigma}(\boldsymbol{u}) = \mathsf{C}\, \boldsymbol{\varepsilon}(\boldsymbol{u}) & \text{in } \Omega \times (0, T], \\ \boldsymbol{u} = \boldsymbol{0} & \text{on } \Gamma_D \times (0, T], \\ \boldsymbol{\sigma}(\boldsymbol{u})\, \boldsymbol{n} = \boldsymbol{0} & \text{on } \Gamma_N \times (0, T], \\ \boldsymbol{u} = \boldsymbol{u}_0 & \text{at } \Omega \times \{0\}, \\ \partial_t \boldsymbol{u} = \boldsymbol{v}_0 & \text{at } \Omega \times \{0\}, \end{cases} \tag{5}$$

where $\boldsymbol{u}_0$ and $\boldsymbol{v}_0$ are the initial conditions. The next result ensures the well-posedness of the corresponding weak formulation of (5). The proof follows closely the one presented in (Raviart et al., 1983, Chapter 8). Next, the vector space $\boldsymbol{H}^1_{0,\Gamma_D}(\Omega)$ stands for the functions in $\boldsymbol{H}^1(\Omega)$ that vanish on Γ_D. All other spaces have their usual meanings and $(\cdot, \cdot)_D$ is the L^2 inner-product on an open set $D \subset \mathbb{R}^d$.

Theorem 1. *Let Ω be a bounded and connected open set with Lipschitz boundary. Suppose $\rho \in L^\infty(\Omega)$ and there exists $\rho_0 \geqslant 0$ such that $\rho(\boldsymbol{x}) > \rho_0$ for a.e. (almost every) $\boldsymbol{x}$ in Ω. Given $\boldsymbol{u}_0 \in \boldsymbol{H}^1_{0,\Gamma_D}(\Omega)$, $\boldsymbol{v}_0 \in \boldsymbol{L}^2(\Omega)$ and $\boldsymbol{f} \in \boldsymbol{L}^2(0,T;\boldsymbol{L}^2(\Omega))$, there exists a unique function $\boldsymbol{u}$ in $C(0,T;\boldsymbol{H}^1_{0,\Gamma_D}(\Omega)) \cap C^1(0,T;\boldsymbol{L}^2(\Omega))$ that satisfy the variational equation, for all $t \in (0,T]$,*

$$d_{tt}(\rho\boldsymbol{u},\boldsymbol{w})_\Omega + (\boldsymbol{\sigma}(\boldsymbol{u}),\boldsymbol{\varepsilon}(\boldsymbol{w}))_\Omega = (\boldsymbol{f},\,\boldsymbol{w})_\Omega, \qquad \forall \boldsymbol{w} \in \boldsymbol{H}^1_{0,\Gamma_D}(\Omega)\,, \tag{6}$$

with $\boldsymbol{u}(0) = \boldsymbol{u}_0$ and $d_t\boldsymbol{u}(0) = \boldsymbol{v}_0$.

3 AN EQUIVALENT GLOBAL-LOCAL FORMULATION

Now, instead of working directly with problem (6), we adopt the following perspective: we seek $\boldsymbol{u}$ as the solution of the elastodynamic model (6) in a weaker, broken space which relaxes continuity and localizes computations. Ultimately, we find that the approach allows for the construction of $\boldsymbol{u}$ using local problems.

From this perspective, we first partition the space-time domain $\Omega \times [0,T]$. We discretize the time interval $[0,T]$ in $n_T + 1$ points $0 = t_0 < t_1 ... < t_{N-1} < t_{n_T} = T$, with $n_T \in \mathbb{N}^*$, (not necessarily) equally distributed, define $I_n := [t_{n-1}, t_n]$ and collect them in the set $\mathcal{T}_n$, where $\Delta t := \max_{n=1,\ldots,n_T} |I_n|$. The partition of the space domain Ω can be general. However, we focus here on partitions based on a family of regular meshes $\{\mathcal{T}_H\}_{H>0}$, where H is the characteristic length of $\mathcal{T}_H$. The mesh can be very general, composed of heterogeneous element geometries. Hereafter, we adopt the terminology employed for three-dimensional domains. Each element K has a boundary ∂K consisting of faces F, and we collect in $\partial\mathcal{T}_H$ the boundaries ∂K, and in $\mathcal{E}_H$ the faces associated with $\mathcal{T}_H$. To each $F \in \mathcal{E}_H$, we associate a normal $\boldsymbol{n}$, taking care to ensure this is facing outward on $\partial\Omega$ for each $F \in \mathcal{E}_H$. For each $K \in \mathcal{T}_H$, we further denote by $\boldsymbol{n}^K$ the outward normal on ∂K, and let $\boldsymbol{n}^K_F := \boldsymbol{n}^K|_F$ for each $F \subset \partial K$. We denote by n_E and n_F the total number of elements and faces in $\mathcal{T}_H$, respectively, and by n^K_F the total number of faces of $K \in \mathcal{T}_H$. See Figure 1 for an illustration.

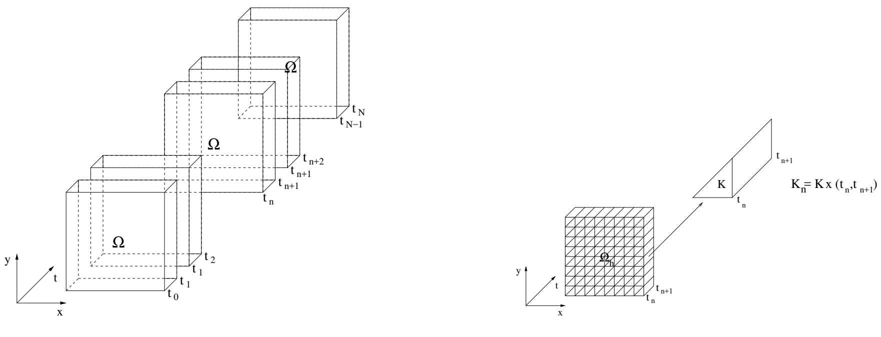

Figure 1: Space-time discretization.

On top of such a discretization, we define the following broken space for the displacement variable

$$\mathbf{V} := \left\{ \boldsymbol{w} \in \boldsymbol{L}^2(\Omega) \,:\, \boldsymbol{w}|_K \in \boldsymbol{H}^1(K) \quad \forall K \in \mathcal{T}_H \right\}, \tag{7}$$

which is a Hilbert space with the following scalar product

$$(\boldsymbol{w},\boldsymbol{v})_{\mathcal{T}_H} := \sum_{K\in\mathcal{T}_H}(\boldsymbol{w},\boldsymbol{v})_K + (\nabla\boldsymbol{w},\nabla\boldsymbol{v})_K \quad \forall \boldsymbol{w},\, \boldsymbol{v}\in\mathbf{V}, \tag{8}$$

and we denote the induced norm by $\|\cdot\|_{\mathbf{V}}$. Also, we define the space of tractions $\boldsymbol{\Lambda}$ given by

$$\boldsymbol{\Lambda} := \left\{\boldsymbol{\tau}\boldsymbol{n}^K|_{\partial K},\, \forall K\in\mathcal{T}_H \,:\, \boldsymbol{\tau}\in H_{0,\Gamma_N}(\mathbf{div};\Omega;\mathbb{S})\right\}, \tag{9}$$

where $H_{0,\Gamma_N}(\mathbf{div};\Omega;\mathbb{S})$ is the space of symmetric matrix functions in $H(\mathbf{div};\Omega;\mathbb{S})$ with vanishing normal component on Γ_N. It is a Banach space when equipped with the following quotient norm

$$\|\boldsymbol{\mu}\|_{\boldsymbol{\Lambda}} := \inf_{\substack{\boldsymbol{\tau}\in H(\mathbf{div};\Omega;\mathbb{S})\\ \boldsymbol{\tau}\boldsymbol{n}^K|_{\partial K}=\boldsymbol{\mu},\forall K\in\mathcal{T}_H}} \|\boldsymbol{\tau}\|_{\mathrm{div}}.$$

We denote by $(\cdot,\,\cdot)_{\mathcal{T}_H}$ and $(\cdot,\,\cdot)_{\partial\mathcal{T}_H}$ the summation of the respective inner (or dual) products over the sets K and ∂K, respectively, given by

$$(\boldsymbol{w},\boldsymbol{v})_{\mathcal{T}_H} := \sum_{K\in\mathcal{T}_H}\int_K \boldsymbol{w}\cdot\boldsymbol{v}\,d\boldsymbol{x} \quad \text{and} \quad (\boldsymbol{\mu},\boldsymbol{v})_{\partial\mathcal{T}_H} := \sum_{K\in\mathcal{T}_H}\langle\boldsymbol{\mu},\boldsymbol{v}\rangle_{\partial K}\,,$$

where $\boldsymbol{w},\,\boldsymbol{v}\in\mathbf{V}$ and $\boldsymbol{\mu}\in\boldsymbol{\Lambda}$. Here, $\langle\cdot,\cdot\rangle_{\partial K}$ is uniquely defined via the dual product involving $\boldsymbol{H}^{-1/2}(\partial K)$ and $\boldsymbol{H}^{1/2}(\partial K)$ through

$$\langle\boldsymbol{\mu},\boldsymbol{v}\rangle_{\partial K} := \int_K (\nabla\cdot\boldsymbol{\tau})\cdot\boldsymbol{v}\,d\boldsymbol{x} + \int_K \boldsymbol{\tau} : \nabla\boldsymbol{v}\,d\boldsymbol{x},$$

where $\boldsymbol{\tau}\boldsymbol{n}^K = \boldsymbol{\mu}$ on ∂K, and we denote it by $(\cdot,\cdot)_{\partial K}$ if $\boldsymbol{\mu}\in\boldsymbol{L}^2(\partial K)$.

Owing to these notations and setting

$$\mathcal{D}_n := C(I_n;\mathbf{V})\cap C^1(I_n;\boldsymbol{L}^2(\Omega))\times C(I_n;\boldsymbol{\Lambda})\,, \tag{10}$$

we propose the following hybrid version of elastodynamic problem (6): For all $I_n\in\mathcal{T}_n$, find $(\boldsymbol{u}^n,\,\boldsymbol{\lambda}^n)\in\mathcal{D}_n$ such that

$$\left\{\begin{aligned} d_{tt}(\rho\boldsymbol{u}^n,\boldsymbol{w})_{\mathcal{T}_H} + (\boldsymbol{\sigma}(\boldsymbol{u}^n),\boldsymbol{\varepsilon}(\boldsymbol{w}))_{\mathcal{T}_H} + (\boldsymbol{\lambda}^n,\boldsymbol{w})_{\partial\mathcal{T}_H} = (\boldsymbol{f},\,\boldsymbol{w})_{\mathcal{T}_H}, \quad \forall\boldsymbol{w}\in\mathbf{V},\\ (\boldsymbol{\mu},\boldsymbol{u}^n)_{\partial\mathcal{T}_H} = 0, \quad \forall\boldsymbol{\mu}\in\boldsymbol{\Lambda},\\ \boldsymbol{u}^n(t_{n-1}) = \boldsymbol{u}^{n-1}(t_{n-1}) \quad \text{and} \quad d_t\boldsymbol{u}^n(t_{n-1}) = d_t\boldsymbol{u}^{n-1}(t_{n-1}) \text{ on } \Omega,\\ \boldsymbol{u}^0(0) = \boldsymbol{u}_0 \quad \text{and} \quad d_t\boldsymbol{u}^0(0) = \boldsymbol{v}_0 \quad \text{on } \Omega. \end{aligned}\right. \tag{11}$$

We emphasize that the first two equations in (11) should be read as being valid for all $t\in I_n$ (fixed although arbitrary), and the global solution $(\boldsymbol{u},\boldsymbol{\lambda})$ is defined such that $(\boldsymbol{u},\boldsymbol{\lambda})\,|_{I_n} = (\boldsymbol{u}^n,\boldsymbol{\lambda}^n)$, for all $I_n\in\mathcal{T}_n$, and hereafter we will say that $(\boldsymbol{u},\boldsymbol{\lambda})$ is a solution of (11).

Observe that the variables in (11) belong a priori to a larger space than the solution of the original problem (6). However, the space of Lagrange multipliers imposes $\boldsymbol{H}^1$-conformity on the solution and respects the boundary conditions. Also, problem (11) has a unique solution (in the sense of Theorem 1) where $\boldsymbol{u}$ coincides with the solution of problem (6). These results are summarized next and the proof follows closely the strategy proposed in Raviart and Thomas (1977) and Lanteri et al. (2017).

Lemma 1. *The function* $(\boldsymbol{u}, \boldsymbol{\lambda})$ *is the solution of* (11) *if and only if* $\boldsymbol{u}$ *solves* (6) *in the sense of Theorem 1. Furthermore, it holds*

$$\boldsymbol{\lambda} = -\boldsymbol{\sigma}(\boldsymbol{u})\boldsymbol{n}^K \quad \text{on } (0,T) \times \partial K \,. \tag{12}$$

Now, rather than selecting a pair of finite subspaces of $\mathbf{V} \times \boldsymbol{\Lambda}$ at this point, we rewrite (11) in an equivalent form which is suitable to reduce the statement to a system of locally- and globally-defined problems. Such an approach guides the definition of stable finite subspaces composed of functions which incorporate multiple scales into the basis functions.

First, observe that problem (11) is equivalent, for all $I_n \in \mathcal{T}_n$, to find $(\boldsymbol{u}^n, \boldsymbol{\lambda}^n) \in \mathcal{D}_n$ such that

$$(\boldsymbol{\mu}, \boldsymbol{u}^n)_{\partial\mathcal{T}_H} = 0, \quad \forall \boldsymbol{\mu} \in \boldsymbol{\Lambda}, \tag{13}$$

and

$$\begin{cases} d_{tt}(\rho\boldsymbol{u}^n, \boldsymbol{w})_K + (\boldsymbol{\sigma}(\boldsymbol{u}^n), \boldsymbol{\varepsilon}(\boldsymbol{w}))_K = -\langle\boldsymbol{\lambda}^n, \boldsymbol{w}\rangle_{\partial K} + (\boldsymbol{f}, \boldsymbol{w})_K, \quad \forall \boldsymbol{w} \in \mathbf{V}(K), \\ \boldsymbol{u}^n(t_{n-1}) = \boldsymbol{u}^{n-1}(t_{n-1}) \quad \text{and} \quad d_t\boldsymbol{u}^n(t_{n-1}) = d_t\boldsymbol{u}^{n-1}(t_{n-1}) \quad \text{on } K, \\ \boldsymbol{u}^0(0) = \boldsymbol{u}_0 \quad \text{and} \quad d_t\boldsymbol{u}^0(0) = \boldsymbol{v}_0 \quad \text{on } K, \end{cases} \tag{14}$$

where $\mathbf{V}(K)$ stands for the space of functions in $\mathbf{V}$ restricted to K.

Notice that (14) implies that $\boldsymbol{u}$ can be computed in each element $K \in \mathcal{T}_h$ from $\boldsymbol{f}$ and $\boldsymbol{\lambda}$ once the latter is known. Owing to this property, we can use the linearity of the elastodynamic operator to decompose the displacement variable into the direct sum

$$\boldsymbol{u}^n = \boldsymbol{u}^{n,\boldsymbol{\lambda}} + \boldsymbol{u}^{n,\boldsymbol{f}}, \tag{15}$$

where $\boldsymbol{u}^{n,\boldsymbol{\lambda}}$ and $\boldsymbol{u}^{n,\boldsymbol{f}}$ satisfy the following local initial boundary value problems

$$\begin{cases} d_{tt}(\rho\,\boldsymbol{u}^{n,\boldsymbol{\lambda}}, \boldsymbol{w})_K + (\boldsymbol{\sigma}(\boldsymbol{u}^{n,\boldsymbol{\lambda}}), \boldsymbol{\varepsilon}(\boldsymbol{w}))_K = -\langle\boldsymbol{\lambda}^n, \boldsymbol{w}\rangle_{\partial K} \quad \forall \boldsymbol{w} \in \mathbf{V}(K), \\ \boldsymbol{u}^{n,\boldsymbol{\lambda}}(t_{n-1}) = d_t\boldsymbol{u}^{n,\boldsymbol{\lambda}}(t_{n-1}) = \mathbf{0} \quad \text{on } K, \end{cases} \tag{16}$$

and

$$\begin{cases} d_{tt}(\rho\,\boldsymbol{u}^{n,\boldsymbol{f}}, \boldsymbol{w})_K + (\boldsymbol{\sigma}(\boldsymbol{u}^{n,\boldsymbol{f}}), \boldsymbol{\varepsilon}(\boldsymbol{w}))_K = (\boldsymbol{f}, \boldsymbol{w})_K \quad \forall \boldsymbol{w} \in \mathbf{V}(K), \\ \boldsymbol{u}^{n,\boldsymbol{f}}(t_{n-1}) = \boldsymbol{u}^{n-1}(t_{n-1}), \quad d_t\boldsymbol{u}^{n,\boldsymbol{f}}(t_{n-1}) = d_t\boldsymbol{u}^{n-1}(t_{n-1}) \quad \text{on } K. \end{cases} \tag{17}$$

Owing to characterization (15) and replacing it in (13), we can rewrite the global problem (13) in an equivalent form in which the Lagrange multipliers are the leading variable, i.e., for each $I_n \in \mathcal{T}_n$ and $t \in I_n$, we look for $\boldsymbol{\lambda}^n(t) \in \boldsymbol{\Lambda}$ such that

$$(\boldsymbol{\mu}, \boldsymbol{u}^{n,\boldsymbol{\lambda}})_{\partial\mathcal{T}_H} = -(\boldsymbol{\mu}, \boldsymbol{u}^{n,\boldsymbol{f}})_{\partial\mathcal{T}_H} \quad \forall \boldsymbol{\mu} \in \boldsymbol{\Lambda}\,. \tag{18}$$

Remark 1 The initial boundary value problems (16) and (17) are well-posed following closely Theorem 1. Since $\boldsymbol{u}^{n,\boldsymbol{\lambda}}, \boldsymbol{u}^{n,\boldsymbol{f}} \in C(I_n; \mathbf{V}) \cap C^1(I_n; \boldsymbol{L}^2(\Omega))$, $n = 1 \cdots n_T$, then $\boldsymbol{u}$ belongs to $C(0,T; \mathbf{V}) \cap C^1(0,T; \boldsymbol{L}^2(\Omega))$ from (15) .

4 THE MHM METHOD

The one-level MHM arises from the choice of a finite dimensional space of $\mathcal{C}^0(0, T; \boldsymbol{\Lambda})$ and looking for the approximate solution $\boldsymbol{\lambda}_H(t)$ of $\boldsymbol{\lambda}(t)$ in such a space satisfying (18) at discrete times. By going discrete, problems (16)-(17) and (18) may be decoupled as follows:

- the local problem (16) is responsible for computing the multiscale basis, with its boundary condition $\boldsymbol{\lambda}^n$ replaced by the space-time approximation $\boldsymbol{\lambda}_H^n$;
- the global problem (18) is responsible for the calculation of the degrees of freedom of $\boldsymbol{\lambda}_H^n$, which depend on $I_n \in \mathcal{T}_n$.

As a result, the one-level approximation $\boldsymbol{u}_H$ of $\boldsymbol{u}$ stems from the combination of the multiscale basis functions, the degrees of freedom of $\boldsymbol{\lambda}_H$ and the solution of (17). A detailed description of $\boldsymbol{u}_H$ is the subject of next section.

4.1 First-level discretization

Since $\boldsymbol{\lambda}$ uniquely determines $\boldsymbol{u}^{\boldsymbol{\lambda}}$, it is enough to select a finite dimensional space $\mathcal{Q}_H^{\Delta t}$ of $\mathcal{C}^0(0, T; \boldsymbol{\Lambda})$ in order to discretize problem (18) in space and time. This leads to the one-level MHM method. To this end, we define $\mathbb{P}_0(I_n)$ the space of piecewise constant functions in the time intervals $I_n \in \mathcal{T}_n$, and set the following polynomial spaces

$$\boldsymbol{\Lambda}_H \;=\; \boldsymbol{\Lambda}_l^m \;:=\; \{\boldsymbol{\mu}_H \in \boldsymbol{\Lambda} \,:\, \boldsymbol{\mu}_H|_{\partial K} \in \boldsymbol{\Lambda}_H(K) \quad \text{for all } K \in \mathcal{T}_H\}\,, \tag{19}$$

$$\boldsymbol{\Lambda}_H(K) \;:=\; \left\{\boldsymbol{\mu}_H \,:\, \boldsymbol{\mu}_H|_F \in \mathbb{P}_l^m(F)^d \quad \text{for all } F \in \partial K\right\}. \tag{20}$$

Here, the space $\mathbb{P}_l^m(F)$ is the space of discontinuous polynomial functions on F of degree less than or equal to $l \geq 0$ and defined on an equally spaced partition of F, composed of m elements ($m \geq 1$). In what follows, the space $\boldsymbol{\Lambda}_l$ stands for $\boldsymbol{\Lambda}_l^1$ and $m_{\boldsymbol{\Lambda}} := \dim \boldsymbol{\Lambda}_H$ and $m_{\boldsymbol{\Lambda}}^K := \dim \boldsymbol{\Lambda}_H(K)$. Observe that, given a face $F \subset \partial K_1 \cap \partial K_2$, with $K_1,\ K_2 \in \mathcal{T}_H$, functions $\boldsymbol{\mu}_H \in \boldsymbol{\Lambda}_H$ are such that $\boldsymbol{\mu}_H|_{F\cap\partial K_1} = -\boldsymbol{\mu}_H|_{F\cap\partial K_2}$ from the definition of $\boldsymbol{\Lambda}$ in (9).

Owing to these choices, we set

$$\mathcal{Q}_H^{\Delta t} := \bigoplus_{I_n \in \mathcal{T}_n} \mathbb{P}_0(I_n) \otimes \boldsymbol{\Lambda}_H\,, \tag{21}$$

where $\boldsymbol{\Lambda}_H$ is given in (19), and observe that such a space is nonconforming in $\mathcal{C}^0(0, T; \boldsymbol{\Lambda})$ with respect to the time variable.

Remark 2 The choice (21) corresponds to the simplest space-time element. It is worth mentioning that the simplicity of (21) associated with its second-order accuracy in time (see Section 5) makes the space (21) the best compromise between precision and computational cost. On the other hand, more involved time interpolation choices may be used with the upside that the conformity is recovered. For instance, we can select

$$\boldsymbol{\lambda}_H(t) = \frac{t_n - t}{t_n - t_{n-1}} \boldsymbol{\lambda}_H^{n-1}(t_{n-1}) + \frac{t - t_{n-1}}{t_n - t_{n-1}} \boldsymbol{\lambda}_H^n(t_n) \quad \forall t \in I_n. \tag{22}$$

Such an option will be explore in future works.

Next, the one-level approximated displacement is decomposed as follows

$$\boldsymbol{u}_H^n = \boldsymbol{u}_H^{n,\boldsymbol{\lambda}_H} + \boldsymbol{u}_H^{n,\boldsymbol{f}}, \tag{23}$$

and the one-level MHM method results from the standard Galerkin method applied to (18), i.e., for all $I_n \in \mathcal{T}_n$, find $\boldsymbol{\lambda}_H^n \in \boldsymbol{\Lambda}_H$ such that

$$(\boldsymbol{\mu}_H, \boldsymbol{u}_H^{n,\boldsymbol{\lambda}_H})_{\partial\mathcal{T}_H} = -(\boldsymbol{\mu}_H, \boldsymbol{u}_H^{n,\boldsymbol{f}})_{\partial\mathcal{T}_H} \quad \forall \boldsymbol{\mu}_H \in \boldsymbol{\Lambda}_H\,, \tag{24}$$

where $\boldsymbol{\lambda}_H\,|_{I_n} = \boldsymbol{\lambda}_H^n$. Observe that Problem (24) will be satisfied at n_T times steps (one per time interval I_n). The functions $\boldsymbol{u}_H^{n,\boldsymbol{\lambda}_H}$, $\boldsymbol{u}_H^{n,\boldsymbol{f}}$ satisfy, respectively,

$$\begin{cases} d_{tt}(\rho\, \boldsymbol{u}_H^{n,\boldsymbol{\lambda}_H}, \boldsymbol{w})_K + (\boldsymbol{\sigma}(\boldsymbol{u}_H^{n,\boldsymbol{\lambda}_H}), \boldsymbol{\varepsilon}(\boldsymbol{w}))_K = -(\boldsymbol{\lambda}_H^n, \boldsymbol{w})_{\partial K}, \quad \forall \boldsymbol{w} \in \mathbf{V}(K)\,, \\ \qquad \boldsymbol{u}_H^{n,\boldsymbol{\lambda}_H}(t_{n-1}) = d_t \boldsymbol{u}_H^{n,\boldsymbol{\lambda}_H}(t_{n-1}) = \mathbf{0}\,, \end{cases} \tag{25}$$

and

$$\begin{cases} d_{tt}(\rho\, \boldsymbol{u}_H^{n,\boldsymbol{f}}, \boldsymbol{w})_K + (\boldsymbol{\sigma}(\boldsymbol{u}_H^{n,\boldsymbol{f}}), \boldsymbol{\varepsilon}(\boldsymbol{w}))_K = (\boldsymbol{f},\, \boldsymbol{w})_K, \quad \forall \boldsymbol{w} \in \mathbf{V}(K)\,, \\ \qquad \boldsymbol{u}_H^{n,\boldsymbol{f}}(t_{n-1}) = \begin{cases} \boldsymbol{u}_0, & \text{if } \ n = 0\,, \\ \boldsymbol{u}_H^{n-1}(t_{n-1}) & \text{if } \ n > 0\,, \end{cases} \\ \qquad d_t\boldsymbol{u}_H^{n,\boldsymbol{f}}(t_{n-1}) = \begin{cases} \boldsymbol{v}_0, & \text{if } \ n = 0\,, \\ \boldsymbol{v}_H^{n-1}(t_{n-1}) & \text{if } \ n > 0\,. \end{cases} \end{cases} \tag{26}$$

Again, problems (25)-(26) should be read as being valid for all $t \in I_n$. It is instructive to consider $\boldsymbol{u}_H^{n,\boldsymbol{\lambda}_H}$ in more detail.

Let $\{\boldsymbol{\psi}_i\}_{i=1}^{m_{\boldsymbol{\Lambda}}}$ be a basis for $\boldsymbol{\Lambda}_H$. Set $\{\boldsymbol{\psi}_i\, \mathbb{1}_{I_n}\}$, with $(i,n) \in \{1, ..., \dim \boldsymbol{\Lambda}_H\} \times n_T$, a basis for $\mathcal{Q}_H^{\Delta t}$, where $\mathbb{1}_{I_n}$ stands for the characteristic function of $I_n \in \mathcal{T}_n$. If $\lambda_i^n \in \mathbb{R}$ are the corresponding degrees of freedom associated to the basis of $\mathcal{Q}_H^{\Delta t}$, then we write

$$\boldsymbol{\lambda}_H^n = \sum_{i=1}^{\dim \boldsymbol{\Lambda}_H} \lambda_i^n\, \boldsymbol{\psi}_i \quad n = 1, ..., n_T. \tag{27}$$

We recall that $\boldsymbol{\psi}_i$ changes its sign according to the sign of $\boldsymbol{n}_F^K \cdot \boldsymbol{n}$, for each $F \subset \partial K$. Let $\boldsymbol{\psi}_j^K$ be the restriction of $\boldsymbol{\psi}_i$ to K, where j has to be understood as a local numbering with respect to K with an one-to-one correspondence to i. We define the set $\boldsymbol{\eta}_i^n \subset \mathcal{D}_n$ such that its local counterpart $\boldsymbol{\eta}_j^{n,K} \subset \mathcal{D}_n$, with $j \in \{1, ..., m_{\boldsymbol{\Lambda}}^K\}$, satisfies the following elastodynamic problem, for all $K \times I_n \in \mathcal{T}_h \times \mathcal{T}_n$,

$$d_{tt}(\rho\, \boldsymbol{\eta}_j^{n,K}, \boldsymbol{w})_K + (\boldsymbol{\sigma}(\boldsymbol{\eta}_j^{n,K}), \boldsymbol{\varepsilon}(\boldsymbol{w}))_K = -(\boldsymbol{\psi}_j^K, \boldsymbol{w})_{\partial K}, \quad \text{for all } \boldsymbol{w} \in \mathbf{V}(K), \tag{28}$$

where $(\boldsymbol{\eta}_j^{n,K}(t_{n-1}), d_t\boldsymbol{\eta}_j^{n,K}(t_{n-1})) = (\mathbf{0}, \mathbf{0})$. As a result of (23) and (27), we write $\boldsymbol{u}_H^n$ on each $I_n \in \mathcal{T}_n$ as follows

$$\boldsymbol{u}_H^n = \sum_{i=1}^{m_{\boldsymbol{\Lambda}}} \lambda_i^n\, \boldsymbol{\eta}_i^n + \boldsymbol{u}_H^{n,\boldsymbol{f}}. \tag{29}$$

The one-level approach assumes that closed formulas are available for $\boldsymbol{\eta}_i^{n,K}$ and $\boldsymbol{u}_H^{n,\boldsymbol{f}}$. As such, to compute (29) effectively, it remains to obtain the degrees of freedom λ_i^n. To this end, we use the face-based global formulation (24) evaluated on n_T discrete time-steps (one per time slab I_n). Indeed, replacing (29) in (24) it follows that λ_i^n, for $i \in \{1, ..., m_{\boldsymbol{\Lambda}}\}$ and $n = 1, ..., n_T$, satisfy the following discrete system

$$\sum_{i=1}^{m_{\boldsymbol{\Lambda}}} \lambda_i^n \, (\boldsymbol{\psi}_j \,, \boldsymbol{\eta}_i^n)_{\partial\mathcal{T}_H} = -(\boldsymbol{\psi}_j \,, \boldsymbol{u}_H^{n,\boldsymbol{f}})_{\partial\mathcal{T}_H} \quad \text{for all } j \in \{1, ..., m_{\boldsymbol{\Lambda}}\} \,,$$

where $\boldsymbol{\eta}_i^n$ and $\boldsymbol{u}_H^{n,\boldsymbol{f}}$ are evaluated at one time per interval $I_n \in \mathcal{T}_n$ (for instance at t_n).

Remark 3 Observe that the one level MHM method is non-conforming in $\boldsymbol{H}^1(\Omega)$ as $\boldsymbol{u}_H$ may be discontinuous across faces, for all $t \in (0, T)$. On the other hand, it is a $H(\mathbf{div}; \Omega; \mathbb{S})$-conforming method as $\boldsymbol{\sigma}(\boldsymbol{u}_H)$ is a symmetric tensor with continuous normal component across faces by construction. Also, the numerical approximations $\boldsymbol{u}_H$ an $d_t\boldsymbol{u}_H$ are strongly continuous in time.

The one level MHM method is generally not feasible, meaning a second level of discretization is necessary to make the method practical. This is the subject of the next section.

4.2 Second-level discretization

We discretize local problems (25)-(26) with respect to the space variable first, by selecting a local finite dimensional space $\mathbf{V}_h(K)$ whose functions are defined over a regular partition of K, denoted by $\left\{\mathcal{T}_h^K\right\}_{h>0}$. Such a partition may differ in each $K \in \mathcal{T}_h$ and h denotes the characteristic length of $\mathcal{T}_h^K$. The global finite dimensional space is then given by

$$\mathbf{V}_h := \bigoplus_{K \in \mathcal{T}_h} \mathbf{V}_h(K), \tag{30}$$

and on top of (30) a second level numerical method is proposed. First observe that the MHM algorithm is quite general, and different numerical methods may be used. In this work, we adopt the Galerkin method on the standard piecewise continuous polynomial space in each element $K \in \mathcal{T}_h$, i.e., $\mathbf{V}_h(K) \subset \mathbf{V}(K)$ is given by

$$\mathbf{V}_h(K) := \left\{\boldsymbol{v}_h \in C(\overline{\Omega}) \,:\, \boldsymbol{v}_h\,|_\tau \in [\mathbb{M}^k(\tau)]^d \quad \text{for all } \tau \in \mathcal{T}_h^K\right\}, \tag{31}$$

where $\mathbb{M}^k(\tau) = \mathbb{P}^k(\tau)$ is the space of polynomial functions on τ of degree less than or equal to $k \geq 1$, or $\mathbb{M}^k(\tau) = \mathbb{Q}^k(\tau)$ is the tensor polynomial space of order at most $k \geq 1$.

As such, the global problem reads: For all $I_n \in \mathcal{T}_n$, find $\boldsymbol{\lambda}_H^n \in \boldsymbol{\Lambda}_H$ such that

$$(\boldsymbol{\mu}_H, \boldsymbol{u}_h^{n,\boldsymbol{\lambda}_H})_{\partial\mathcal{T}_H} = -(\boldsymbol{\mu}_H, \boldsymbol{u}_h^{n,\boldsymbol{f}})_{\partial\mathcal{T}_H} \quad \forall \boldsymbol{\mu}_H \in \boldsymbol{\Lambda}_H \,, \tag{32}$$

where $\boldsymbol{u}_h^{n,\boldsymbol{\lambda}_H}$ and $\boldsymbol{u}_h^{n,\boldsymbol{f}}$ belong to $\mathbf{V}_h$. They correspond to the second level approximation of $\boldsymbol{u}_H^{n,\boldsymbol{\lambda}_H}$ and $\boldsymbol{u}_H^{n,\boldsymbol{f}}$. As a result, the semi-discrete approximation of the exact solution is given by

$$\boldsymbol{u} \approx \boldsymbol{u}_{H,h} := \boldsymbol{u}_h^{\boldsymbol{\lambda}_H} + \boldsymbol{u}_h^{\boldsymbol{f}}, \tag{33}$$

where, as usual, the global functions in time $\boldsymbol{u}_h^{\boldsymbol{\lambda}_H}$ and $\boldsymbol{u}_h^{\boldsymbol{f}}$ are defined through their local (in time) counterpart $\boldsymbol{u}_h^{n,\boldsymbol{\lambda}_H}$ and $\boldsymbol{u}_h^{n,\boldsymbol{f}}$. They correspond to the solution of the following Galerkin methods: For each $K \in \mathcal{T}_h$, find $\boldsymbol{u}_h^{n,\boldsymbol{\lambda}_H}|_K \in \mathbf{V}_h(K)$, for all $I_n \in \mathcal{T}_n$, such that

$$\begin{cases} d_{tt}(\rho\, \boldsymbol{u}_h^{n,\boldsymbol{\lambda}_H}, \boldsymbol{w}_h)_K + (\boldsymbol{\sigma}(\boldsymbol{u}_h^{n,\boldsymbol{\lambda}_H}), \boldsymbol{\varepsilon}(\boldsymbol{w}_h))_K = -(\boldsymbol{\lambda}_H^n, \boldsymbol{w}_h)_{\partial K}, \quad \text{for all } \boldsymbol{w}_h \in \mathbf{V}_h(K), \\ \boldsymbol{u}_h^{n,\boldsymbol{\lambda}_H}(t_{n-1}) = \mathbf{0}, \\ d_t \boldsymbol{u}_h^{n,\boldsymbol{\lambda}_H}(t_{n-1}) = \mathbf{0}, \end{cases} \tag{34}$$

and find $\boldsymbol{u}_h^{n,\boldsymbol{f}}|_K \in \mathbf{V}_h(K)$ such that

$$\begin{cases} d_{tt}(\rho\, \boldsymbol{u}_h^{n,\boldsymbol{f}}, \boldsymbol{w}_h)_K + (\boldsymbol{\sigma}(\boldsymbol{u}_h^{n,\boldsymbol{f}}), \boldsymbol{\varepsilon}(\boldsymbol{w}_h))_K = (\boldsymbol{f},\, \boldsymbol{w}_h)_K, \quad \text{for all } \boldsymbol{w}_h \in \mathbf{V}_h(K), \\ \boldsymbol{u}_h^{n,\boldsymbol{f}}(t_{n-1}) = \boldsymbol{u}_h^{n-1}(t_{n-1}), \\ d_t \boldsymbol{u}_h^{n,\boldsymbol{f}}(t_{n-1}) = d_t \boldsymbol{u}_h^{n-1}(t_{n-1}), \end{cases} \tag{35}$$

with $\boldsymbol{u}_h^{0,\boldsymbol{f}}(0) = \boldsymbol{u}_{0h}$ and $d_t \boldsymbol{u}_h^{0,\boldsymbol{f}}(0) = \boldsymbol{v}_{0h}$. Here $\boldsymbol{u}_{0h}$ and $\boldsymbol{v}_{0h}$ must be understood as well-chosen projections of the exact initial conditions in the sense that such approximations do not undermine convergence rates. Like in the one-level discretization, the solution of (34) can be decomposed as follows

$$\boldsymbol{u}_h^{n,\boldsymbol{\lambda}_H} = \sum_{i=1}^{m_{\boldsymbol{\Lambda}}} \lambda_i^n\, \boldsymbol{\eta}_{i,h}^n \quad n = 1, ..., n_T,$$

where the local counterpart, $\boldsymbol{\eta}_{i,h}^{n,K}$, of the multiscale basis function $\boldsymbol{\eta}_{i,h}^n$ solves

$$d_{tt}(\rho\, \boldsymbol{\eta}_{i,h}^{n,K}, \boldsymbol{w}_h)_K + (\boldsymbol{\sigma}(\boldsymbol{\eta}_{i,h}^{n,K}), \boldsymbol{\varepsilon}(\boldsymbol{w}_h))_K = -(\boldsymbol{\psi}_i^K, \boldsymbol{w}_h)_{\partial K}, \quad \text{for all } \boldsymbol{w}_h \in \mathbf{V}_h(K), \tag{36}$$

with $(\boldsymbol{\eta}_{i,h}^{n,K}(t_{n-1}), d_t \boldsymbol{\eta}_{i,h}^{n,K}(t_{n-1})) = (\mathbf{0}, \mathbf{0})$.

The two-level MHM method corresponds to the global problem formulation: Find $\boldsymbol{\lambda}_H^n \in \boldsymbol{\Lambda}_H$, for $n = 1, ..., n_T$, such that

$$(\boldsymbol{\mu}_H, \boldsymbol{u}_h^{n,\boldsymbol{\lambda}_H})_{\partial \mathcal{T}_H} = -(\boldsymbol{\mu}_H, \boldsymbol{u}_h^{n,\boldsymbol{f}})_{\partial \mathcal{T}_H} \quad \forall \boldsymbol{\mu}_H \in \boldsymbol{\Lambda}_H, \tag{37}$$

which is evaluated at time steps t_n, $n = 1, ..., n_T$.

In order to prepare (34) (e.g. (36)) and (35) to be discretize in time, we write such problems as a ODE system. To this end, let $\{\boldsymbol{\varphi}_i\}_{i=1}^{m_K}$ be a basis for $\mathbf{V}_h(K)$, $K \in \mathcal{T}_H$, where $m_K = \dim \mathbf{V}_h(K)$. The two-level approximate solutions $\boldsymbol{\eta}_{j,h}^{n,K}$ and $\boldsymbol{u}_h^{n,\boldsymbol{f}}|_K$ in the time interval I_n can be written as

$$\boldsymbol{\eta}_{j,h}^{n,K}(t) := \sum_{i=1}^{m_K} d_{j,i}^{n,K}(t) \boldsymbol{\varphi}_i \quad \text{and} \quad \boldsymbol{u}_h^{n,\boldsymbol{f}}(t) = \sum_{i=1}^{m_K} f_i^{n,K}(t) \boldsymbol{\varphi}_i, \tag{38}$$

where $d_{j,i}^{n,K}, f_i^{n,K} : I_n \to \mathbb{R}$ are defined for $n = 1, ..., n_T$. Thereby, at this stage, the two-level approximation restricted to $K \in \mathcal{T}_H$ reads

$$\boldsymbol{u}_{H,h}^n = \sum_{i=1}^{m_K} \Big(\sum_{j=1}^{m_{\boldsymbol{\Lambda}}^K} \lambda_j^n d_{j,i}^{n,K} + f_i^{n,K} \Big) \boldsymbol{\varphi}_i \quad \text{on } I_n \times K, \tag{39}$$

where λ_j^n are the degrees of freedom of $\boldsymbol{\lambda}_H^n$ restricted to $K \in \mathcal{T}_H$ with local numbering j.

Define Ψ_j a matrix with columns Ψ_j, $j = 1, \cdots, m_{\boldsymbol{\Lambda}}^K$, which represents the coordinate vector field $d_{j,i}^{n,K}$, $i = 1, ..., m_K$. Also, let vector ξ be the coordinate vector field $f_i^{n,K}$, $i = 1, ..., m_K$. Observe that such functions are of class $C^1(I_n)$ in each time interval I_n. Now, replacing (38) in (34)-(35), we arrive at that, for each $K \times I_n$, the local semi-discrete problem reads: Find $\Psi : I_n \to \mathbb{R}^{m_K \times m_{\boldsymbol{\Lambda}}^K}$ and $\xi : I_n \to \mathbb{R}^{m_K}$ such that

$$\begin{cases} M^K \Psi''(t) + R^K \Psi(t) = -Q^K \quad \forall t \in I_n, \\ \Psi_j(t_{n-1}) = \Psi'(t_{n-1}) = 0, \end{cases} \tag{40}$$

and

$$\begin{cases} M^K \xi''(t) + R^K \xi(t) = f^K(t) \quad \forall t \in I_n, \\ \quad \xi(t_{n-1}) = d_K^{n-1} \quad \text{and} \quad \xi'(t_{n-1}) = \dot{d}_K^{n-1}, \end{cases} \tag{41}$$

where $M_{ij}^K := (\rho \boldsymbol{\varphi}_j, \boldsymbol{\varphi}_i)_K$, $R_{ij}^K := (\boldsymbol{\sigma}(\boldsymbol{\varphi}_j), \boldsymbol{\varepsilon}(\boldsymbol{\varphi}_i))_K$, $Q_{ij}^K := (\boldsymbol{\psi}_j^K, \boldsymbol{\varphi}_i)_K$ and $f_i^K(t) := (\boldsymbol{f}(t), \boldsymbol{\varphi}_i)_K$. The vectors $d_K^n, \dot{d}_K^n \in \mathbb{R}^{m_K}$ represent the coordinates of $\boldsymbol{u}_{H,h}^n$ and $\boldsymbol{v}_{H,h}^n$, respectively. Accordingly to (39), the i-component of the vectors d_K^n and $\dot{d}_K^n$ reads

$$(d_K^n)_i = \sum_{j=1}^{m_{\boldsymbol{\Lambda}}^K} \lambda_j^n d_{j,i}^{n,K} + f_i^{n,K} \quad \text{and} \quad (\dot{d}_K^n)_i = \sum_{j=1}^{m_{\boldsymbol{\Lambda}}^K} \lambda_j^n \dot{d}_{j,i}^{n,K} + \dot{f}_i^{n,K}.$$

Now, we head to the time discretization of (40) and (41). To this end, we use the Newmark method (Raviart et al., 1983, Sec. 8.5). The Newmark method yields second order accurate approximation (in time) for the displacement and velocity fields. First, we need some additional notations associated to the (local) time discretization. We decompose I_n in a (non necessary) uniform partition, i.e., $t_n = \tau_n^0 < \tau_n^1 < .... < \tau_n^{n_t} = t_{n+1}$, with $n_t \in N^*$ and $\Delta\tau_n^k = \tau_n^k - \tau_n^{k-1}$, and $k = 1, ..., n_t$, and set $\Delta\tau_n := \max_{k=1,...,n_t} \Delta\tau_n^k$. Observe that such a partition can be set differently in each element $K \in \mathcal{T}_h$, which naturally induces a *local* time stepping scheme. For sake of clarity, we drop such a dependency in the notation. See Figure 2 for an illustration of the second level space-time discretization.

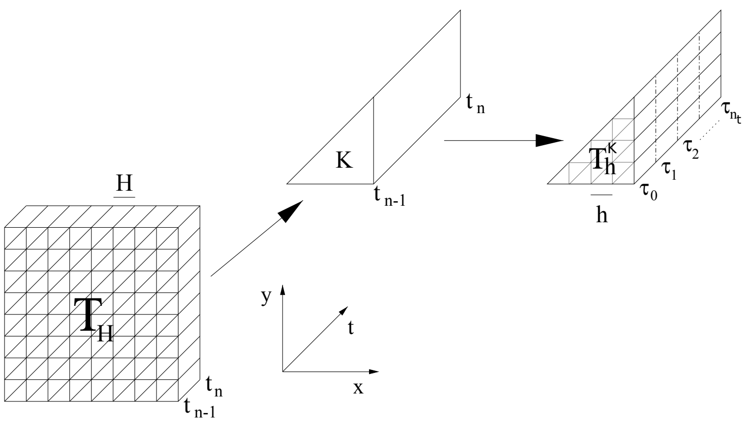

Figure 2: Local space-time domain discretization.

In the context of the MHM method, the Newmark method provides accurate approximations of $\boldsymbol{\eta}_{i,h}^{n,K}$ and $\boldsymbol{u}_h^{n,\boldsymbol{f}}$, and $d_t\boldsymbol{\eta}_{i,h}^{n}$ and $d_t\boldsymbol{u}_h^{n,\boldsymbol{f}}$ in time. To lighten notation, we apply the Newmark method to problems (40) and (41) dropping vectors dependency in terms of K and I_n.

As such, the Newmark scheme applied to local problems Eqs. (40) and (41) leads to: For each $s = 1, \cdots, n_t$, find $\Psi^s, \dot{\Psi}^s \in \mathbb{R}^{m_K \times m_{\boldsymbol{\Lambda}}^K}$ and $\xi^s, \dot{\xi}^s \in \mathbb{R}^{m_K}$ such that

$$\left\{\begin{aligned} \left(M^K + \beta\Delta\tau^2 R^K\right)\xi^s &= M^K\left(\xi^{s-1} + \Delta\tau\dot{\xi}^{s-1}\right) + \Delta\tau^2\left(\beta - \frac{1}{2}\right)R^K\xi^{s-1} + \\ &+ \Delta\tau^2\left(\beta f^K(\tau_s) + \left(\frac{1}{2} - \beta\right)f^K(\tau_{s-1})\right), \\ M^K\dot{\xi}^s &= M^K\dot{\xi}^{s-1} - \Delta\tau R^K\left(\gamma\xi^s + (1-\gamma)\,\xi^{s-1}\right) + \\ &+ \Delta\tau\left(\gamma f^K(\tau_s) + (1-\gamma)\,f^K(\tau_{s-1})\right), \end{aligned}\right. \tag{42}$$

where $\xi^s \approx \xi(\tau_s)$ and $\dot{\xi}^s \approx \xi'(\tau_s)$, for all $s = 1, ..., n_t$, and

$$\left\{\begin{aligned} \left(M^K + \beta\Delta\tau^2 R^K\right)\Psi^s &= M^K\left(\Psi^{s-1} + \Delta\tau\dot{\Psi}^{s-1}\right) + \Delta\tau^2\left(\beta - \frac{1}{2}\right)R^K\Psi^{s-1} - \frac{\Delta\tau^2}{2}Q^K, \\ M^K\dot{\Psi}^s &= M^K\dot{\Psi}^{s-1} - \Delta\tau R^K\left(\gamma\Psi^s + (1-\gamma)\,\Psi^{s-1}\right) - \Delta\tau Q^K, \end{aligned}\right. \tag{43}$$

where $\Psi^s \approx \Psi(\tau_s)$ and $\dot{\Psi}^s \approx \Psi'(\tau_s)$, for all $s = 1, ..., n_t$. The initial conditions are $\Psi^0 = \dot{\Psi}^0 = 0$, $\xi^0 = d_K^{n-1}$ and $\dot{\xi}^0 = \dot{d}_K^{n-1}$, and α and β are positive parameters.

The final local marching process ($s = n_t$) provides the functions $\boldsymbol{\eta}_{j,h}^{n,K}$ and $\boldsymbol{u}_h^{n,\boldsymbol{f}}$ at time step t_n needed to solve (37). They are given as follows

$$\boldsymbol{\eta}_{j,h}^{n,K}(t_n) := \sum_{i=1}^{m_K} \Psi_{ij}^{n_t}\boldsymbol{\varphi}_i \quad \text{and} \quad \boldsymbol{u}_h^{n,\boldsymbol{f}}(t_n) := \sum_{i=1}^{m_K} \xi_i^{n_t}\boldsymbol{\varphi}_i, \tag{44}$$

as well as theirs time derivatives

$$\dot{\boldsymbol{\eta}}_{j,h}^{n,K}(t_n) := \sum_{i=1}^{m_K} \dot{\Psi}_{ij}^{n_t}\boldsymbol{\varphi}_i \quad \text{and} \quad \dot{\boldsymbol{u}}_h^{n,\boldsymbol{f}}(t_n) := \sum_{i=1}^{m_K} \dot{\xi}_i^{n_t}\boldsymbol{\varphi}_i. \tag{45}$$

We are ready to present the fully discrete problem which corresponds to solve (37) using (44). In its matricial form, problem (37) corresponds to find $\lambda^n \in \mathbb{R}^{m_{\boldsymbol{\Lambda}}}$ such that, for each $n = 1, \cdots, n_T$, it holds

$$A^n\lambda^n = -F^n, \tag{46}$$

where $A_{ij}^n := (\boldsymbol{\psi}_i, \boldsymbol{\eta}_{j,h}^n(t_n))_{\partial\mathcal{T}_H}$, and $F_i^n := (\boldsymbol{\psi}_i, \boldsymbol{u}_h^{n,\boldsymbol{f}}(t_n))_{\partial\mathcal{T}_H}$.

Finally, the two-level approximation of the exact displacement $\boldsymbol{u}$ and velocity $\boldsymbol{v}$ at time steps t_n, $n = 1, \cdots, n_T$, and restricted to $K \in \mathcal{T}_h$, are given as follows

$$\boldsymbol{u}_{H,h}^n(t_n) = \sum_{i=1}^{m_K}\left(\sum_{j=1}^{m_{\boldsymbol{\Lambda}}^K}\lambda_j^n\, d_{j,i}^{n,K} + f_i^{n,K}\right)\boldsymbol{\varphi}_i \tag{47}$$

and

$$\boldsymbol{v}_{H,h}^n(t_n) = \sum_{i=1}^{m_K}\left(\sum_{j=1}^{m_{\boldsymbol{\Lambda}}^K}\lambda_j^n\, \dot{d}_{j,i}^{n,K} + \dot{f}_i^{n,K}\right)\boldsymbol{\varphi}_i. \tag{48}$$

4.3 Algorithmic aspects

Define the following element-wise local contributions

$$\begin{aligned}
&A^K = (a_{ij}^K) \in \mathbb{R}^{m_{\mathbf{\Lambda}}^K \times m_{\mathbf{\Lambda}}^K} \qquad \text{with } a_{ij}^K := (\boldsymbol{\psi}_i^K, \boldsymbol{\eta}_{j,h}^{n,K})_{\partial K} \quad 1 \leqslant i,j \leqslant m_{\mathbf{\Lambda}}^K, \\
&F_K^n = (F_{K,i}^n) \in \mathbb{R}^{m_{\mathbf{\Lambda}}^K} \qquad \text{with } F_{K,i}^n := (\boldsymbol{\psi}_i^K, \boldsymbol{u}_h^{\boldsymbol{f},n})_{\partial K} \quad 1 \leqslant i \leqslant m_{\mathbf{\Lambda}}^K,
\end{aligned} \tag{49}$$

and let A^n and F^n be obtained by assembling the local terms (49).

Hereafter, we assume that the time partition is equally-spaced. In such a case, the multiscale basis functions can be computed once and for all since $\boldsymbol{\eta}_{j,h}^{n,K} = \boldsymbol{\eta}_{j,h}^{1,K}$ and $\dot{\boldsymbol{\eta}}_{j,h}^{n,K} = \dot{\boldsymbol{\eta}}_{j,h}^{1,K}$ for all $n, j \geqslant 1$ and $K \in \mathcal{T}_H$. We then denote these two different terms, in each element K, by $\boldsymbol{\eta}_{j,h}^K$ and $\dot{\boldsymbol{\eta}}_{j,h}^K$. It is worth of pointing out that the multiscale basis functions $\boldsymbol{\eta}_{j,h}^K$ and $\boldsymbol{u}_h^{n,\boldsymbol{f}}|_K$ can be computed in parallel since they satisfy independent local problems. Also, it turns out that the global matrix $A = A^n$ can be factorized just once when a direct linear solver is adopted and the physical coefficients are independent of the time step.

Next, we present the MHM algorithm which is split into two parts mimicking the MHM's structure. The global part is introduced in Algorithm 1 and the local one in Algorithm 2.

Algorithm 1 MHM Algorithm - Global Problem

for $n = 1, \cdots, n_T$ **do**
  for all $K \in \mathcal{T}_h$ **do**
    if $n = 1$ **then**
      Compute the local solutions $\boldsymbol{\eta}_{j,h}^K$ and $\dot{\boldsymbol{\eta}}_{j,h}^K$ (see Algorithm 2)
      Compute the local term A^K
      Assemble A^K in A and factorize it
    end if
    Compute the local solutions $\boldsymbol{u}_h^{n,\boldsymbol{f}}|_K$ and $\dot{\boldsymbol{u}}_h^{n,\boldsymbol{f}}|_K$ (see Algorithm 2)
    Compute the local terms F_K^n
    Assemble F_K^n in F^n
  end for
  Solve the global linear system

$$A\,\lambda^n = -F^n \tag{50}$$

  Compute the global solutions

$$\boldsymbol{u}_{H,h}^n = \sum_{i=1}^{m_{\mathbf{\Lambda}}} \lambda_i^n\, \boldsymbol{\eta}_{i,h} + \boldsymbol{u}_h^{n,\boldsymbol{f}} \quad \text{and} \quad \boldsymbol{v}_{H,h}^n = \sum_{i=1}^{m_{\mathbf{\Lambda}}} \lambda_i^n\, \dot{\boldsymbol{\eta}}_{i,h} + \dot{\boldsymbol{u}}_h^{n,\boldsymbol{f}}. \tag{51}$$

end for

Algorithm 2 MHM Algorithm - Local Problems

if $n = 1$ **then**
  Compute M^K, R^K and Q^K
  Factorize matrices M^K and $M^K + \beta \Delta\tau^2 R^K$
  Set $\Psi^0 = \dot{\Psi}^0 = 0 \in \mathbb{R}^{m_K \times m_\Lambda^K}$
  for $s = 1, \cdots, n_t$ **do**
    Solve system (40)
  end for
  Compute the local solutions

$$\boldsymbol{\eta}_{j,h}^K = \sum_{i=1}^{m_K} \Psi_{ij}^{n_t} \boldsymbol{\varphi}_i \qquad \text{and} \qquad \dot{\boldsymbol{\eta}}_{j,h}^K = \sum_{i=1}^{m_K} \dot{\Psi}_{ij}^{n_t} \boldsymbol{\varphi}_i$$

  Compute the local term

$$A^K = (Q^K)^T\, \Psi^{n_t}$$

end if
Set $\xi^0 = d_K^{n-1}$ and $\dot{\xi}^0 = \dot{d}_K^{n-1}$.
for $s = 1, \cdots, n_t$ **do**
  Compute f^K
  Solve system (41)
end for
Compute the local solutions

$$\boldsymbol{u}_h^{n,\boldsymbol{f}}|_K = \sum_{i=1}^{m_K} \xi_i^{n_t} \boldsymbol{\varphi}_i \qquad \text{and} \qquad \dot{\boldsymbol{u}}_h^{n,\boldsymbol{f}}|_K = \sum_{i=1}^{m_K} \dot{\xi}_i^{n_t} \boldsymbol{\varphi}_i$$

Compute the local term

$$F_K^n = (Q^K)^T\, \xi^{n_t}$$

5 NUMERICAL EXPERIMENTS

In this section, we validate theoretical aspects of MHM method using a first three-dimensional test with analytical solution. Next, a problem with highly heterogeneous coefficients is considered in a two-dimensional domain to assess the upscalling feature of the MHM method. Numerical experiments assume that the elastic media is isotropic. In other words, the tensor C is characterized by the Lamé coefficients μ and ν as follows

$$\mathsf{C}_{ijkl} := 2\,\mu\,\delta_{ik}\,\delta_{jl} + \nu\delta_{ij}\,\delta_{kl} \quad \text{or} \quad \mathsf{C}\,\boldsymbol{\varepsilon} = 2\,\mu\,\boldsymbol{\varepsilon} + \nu\,\mathrm{tr}(\boldsymbol{\varepsilon})\,I, \tag{52}$$

where δ_{ij} denotes the Kronecker's delta, $\mathrm{tr}(\boldsymbol{\varepsilon})$ represents the trace of $\boldsymbol{\varepsilon}$ and I is the identity tensor. The multiscale struture of the media will impact the coefficients ρ, μ and ν.

The triangular and tetrahedron meshes are generated using the softwares Triangle Shewchuk (1996) and TetGen Si (2015), respectively.

5.1 An analytical problem

The elastodynamic problem is defined in a unit cube with Lamé coefficients $\mu = 0.4$ and $\nu = 0.4$, and density $\rho = 1$. The exact solution $\boldsymbol{u} = [u_1, u_2, u_3]^T$ is given by

$$\begin{cases} u_1(t,x,y,z) & = \frac{1}{2}(1-\cos(\omega t))\sin(2\pi x)\sin(2\pi y)\sin(2\pi z)\,, \\ u_2(t,x,y,z) & = -\frac{1}{2}(1-\cos(\omega t))\sin(2\pi x)\sin(2\pi y)\sin(2\pi z)\,, \\ u_3(t,x,y,z) & = \frac{1}{2}(1-\cos(\omega t))\sin(\pi x)\sin(\pi y)\sin(\pi z)\,, \end{cases} \tag{53}$$

where $\omega = \sqrt{2\mu\rho^{-1}}\pi$. The Dirichlet boundary conditions on $\partial\Omega$ and $\boldsymbol{f}$ are computed accordingly. Homogeneous initial conditions are applied. We set $l = k+2$ in the definition of the interpolation spaces $\boldsymbol{\Lambda}_H = \boldsymbol{\Lambda}_l$ and $\mathbf{V}_h$, and study the convergence aspects of the numerical solutions with respect to H and Δt. For simplicity, no local time step is used (i.e., $\Delta\tau = \Delta t$).

The convergence history are measured in $\boldsymbol{L}^2(\Omega)$ and $\boldsymbol{H}^1(\mathcal{T}_H)$ norms for displacement and velocity, and in the $H(\mathbf{div};\Omega;\mathbb{S})$-broken norm, i.e.,

$$\|\boldsymbol{\sigma}\|_{\text{div}} := \sqrt{\sum_{K\in\mathcal{T}_H}\sum_{\tau\in\mathcal{T}_h^K}\|\boldsymbol{\sigma}\|_{0,\tau}^2 + \|\nabla\cdot\,\boldsymbol{\sigma}\|_{0,\tau}^2}, \tag{54}$$

for the stress. Also, we measure the total (discrete) energy E_{Hh}^n for long-time simulations through the following formula

$$E_{Hh}^n := \frac{1}{2}\sum_{K\in\mathcal{T}_h}\left[\int_K \rho\,\boldsymbol{v}_{H,h}^n\cdot\boldsymbol{v}_{H,h}^n + \int_K \mathsf{C}\,\boldsymbol{\varepsilon}(\boldsymbol{u}_{H,h}^n):\boldsymbol{\varepsilon}(\boldsymbol{u}_{H,h}^n)\right] \quad \text{for } n = 1,...,n_T. \tag{55}$$

We observe in Figure 3 that the proposed MHM method is second order convergent in terms of Δt and achieves superconvergence with respect to H. Such a superconvergence was theoretically proved for the elastostatic case in (Harder and Valentin, 2016). It worth of mentioning that the adoption of Newmark method leads to convergent numerical solutions for both displacement and velocity. Specifically, we found errors of $O(H^{\ell+2})$ in the $\boldsymbol{L}^2(\Omega)$ norm and $O(H^{\ell+1})$ using the $\boldsymbol{H}^1(\mathcal{T}_H)$ norm. Also interestingly, we found superconvergent stress approximation of $O(H^{\ell})$ in the $H(\mathbf{div};\Omega;\mathbb{S})$-broken norm.

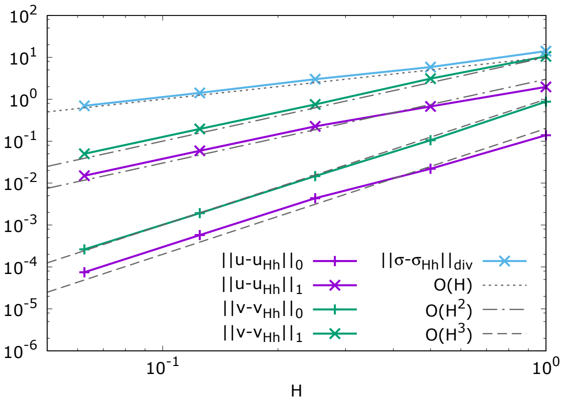

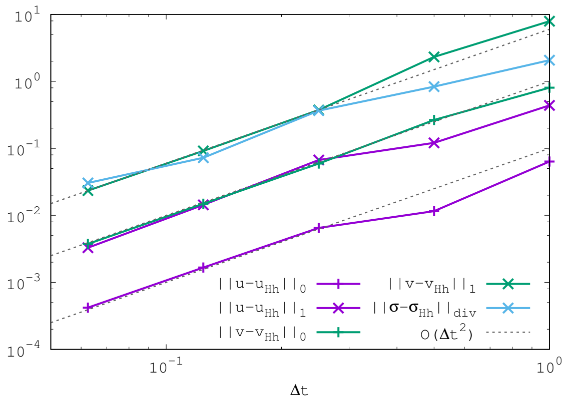

Figure 3: Convergence history with respect to H (left) and Δt (right). Here $\boldsymbol{\Lambda}_H = \boldsymbol{\Lambda}_1$.

We depict the isosurfaces of $|\boldsymbol{u}_{H,h}|$ in Figure 4 at the times steps 0.5, 1 and 1.5, and $x = 0.25$ using $\boldsymbol{\Lambda}_H = \boldsymbol{\Lambda}_1^{16}$. Also observe in Figure 4 that energy (55) stays bounded (with no dissipation). This shows that the present MHM method conserves the total energy of the system in long-term simulations.

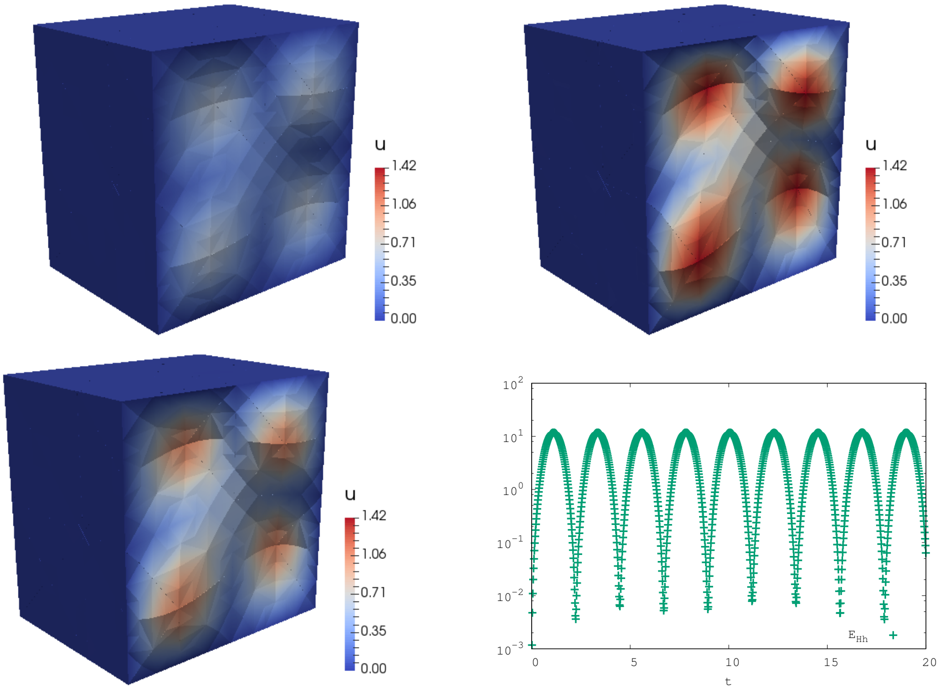

Figure 4: Isosurfaces of $|\boldsymbol{u}_{H,h}|$ at three time steps (top and bottom on the left). The total energy history (bottom on the right).

5.2 Multiscale experiments

The HPC4E Seismic Test Suite presented in de la Puente (2016) is used for validating the MHM method. The original computational domain from this test suite is a three-dimensional box split in 16 horizontal layers. The top layer determines the topography and the bottom layer ends in a plane $4,480.78$ m depth, as shown in Figure 5. The depth is positive downwards and zero represents the sea level. The coefficients are constant inside each layer, as we see in Figure 5.

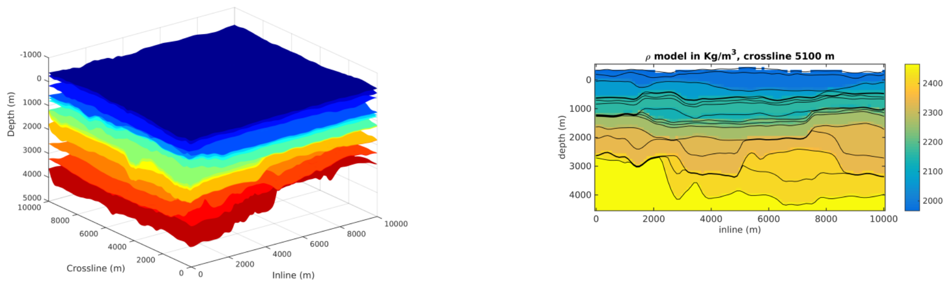

Figure 5: The physical domain divided in layers (left) and a vertical cut showing the density ρ (right). Adapted from de la Puente (2016).

The multiscale feature of the Lamé coefficients is provided by the highly accurate definition of the interfaces (horizons) between adjacent layers. In de la Puente (2016), the elastic media is characterized by three parameters: density ρ, compressional velocity v_p and shear velocity v_s. This is a common characterization in wave propagation problems. We recover μ and ν using the following relationships

$$\mu = \rho\, v_s^2 \quad \text{and} \quad \nu = \rho\,(v_p^2 - v_s^2). \tag{56}$$

From (de la Puente, 2016, Table 1), we use the upper layers 1^*, 2^* and 3^*, which are the positive truncation of the original layers 1, 2 and 3, so that the domain fits perfectly in the box $[500\text{ m}, 450\text{ m}]$. Here, we propose a two-dimensional version of the aforementioned problem using homogeneous Neumann boundary condition on the boundary. The y-axis represents the depth and the x-axis represents the in-line component. The source function $\boldsymbol{f} = [f_1, f_2]^T$ is a concentrated load located at $\boldsymbol{x_f} = [500\text{ m}, 50\text{ m}]^T$ and defined by

$$\boldsymbol{f}(\boldsymbol{x}, t) = \begin{cases} f_{shot}(t)\,\frac{\boldsymbol{x}-p_{shot}}{|\boldsymbol{x}-p_{shot}|}, & 0 < |\boldsymbol{x} - p_{shot}| < r_{shot} \text{ and } t < t_{shot}, \\ \{0,0\}, & \text{other cases}, \end{cases}, \tag{57}$$

where t_{shot}, p_{shot} and r_{shot} are, respectively, the time duration, the point of application and the radius of the shot; and $f_{shot}(t)$ is the intensity of the shot, modeled by an Ormsby wavelet.

A simplified model containing layers 1^*, 7 and 15 from (de la Puente, 2016, Table 1) is set to validate the MHM method in non-aligned meshes. A coarse non-structured mesh is adopted with 341 triangular elements. The edges of the mesh are not aligned with the layer interfaces as shown in Figure 6 (left). We set $\boldsymbol{\Lambda}_H = \boldsymbol{\Lambda}_2^8$ on edges and use a sub-mesh with 64 $\mathbb{P}^3$ elements. The final time $T = 0.3$ and $\Delta t = 10^{-3}$. We depict in Figure 6 (right) and Figure 7 the isovalues of $|\boldsymbol{u}_{H,h}|$ at three different time steps. We observe that the solution is perfectly captured even though interfaces do not coincide with edges.

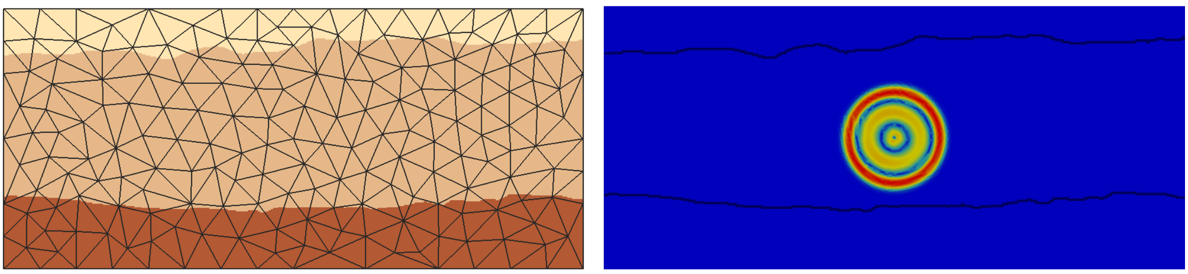

Figure 6: Domain with three layers with a non-aligned unstructured mesh (left). Isovalues of $|\boldsymbol{u}_{H,h}|$ at $t = 0.05$ (right).

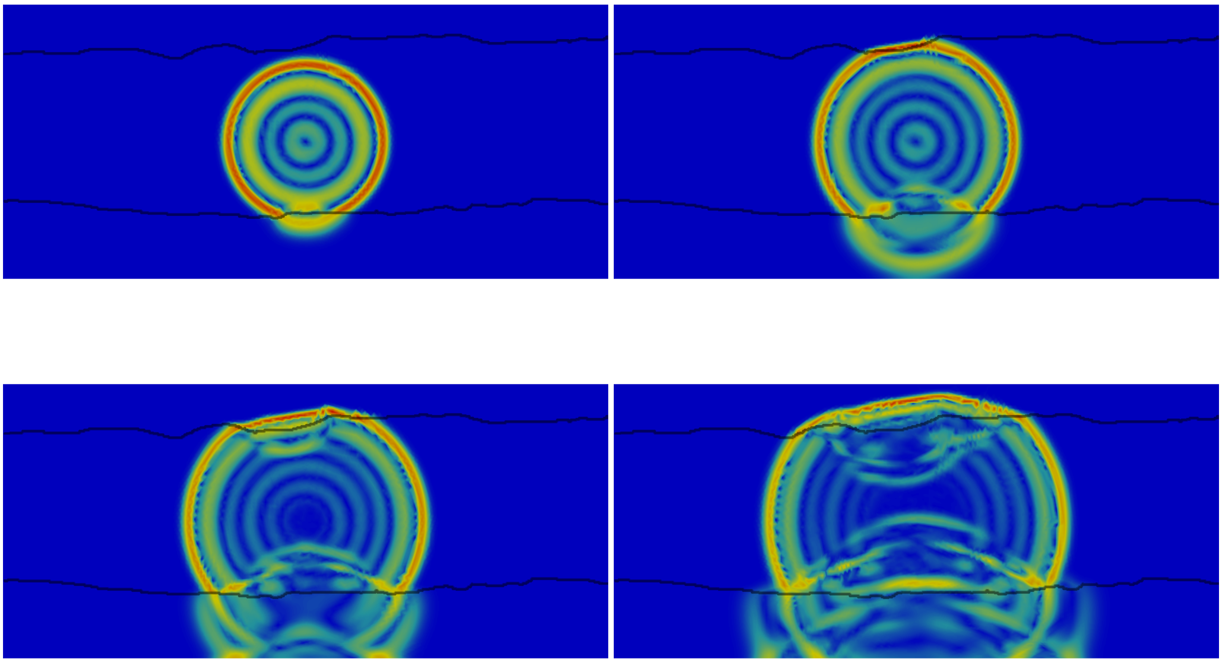

Figure 7: Isovalues of $|\boldsymbol{u}_{H,h}|$ at $t = 0.08$, $t = 0.1$, $t = 0.12$ and $t = 0.15$.

Next, we compare the solutions from the MHM method with a reference solution using the 16-layer problem. Again, the coarse non-structured mesh with 341 triangular elements is adopted for the MHM case. We set $\mathbf{\Lambda}_H = \mathbf{\Lambda}_1^4$ on edges and use a sub-mesh with $4,096$ $\mathbb{P}^3(\tau)$ elements. The final time $T = 1$ and $\Delta t = 5 \times 10^{-3}$. The reference solution is obtained from the standard Galerkin method on a mesh with $90,232$ $\mathbb{P}^3(K)$ elements and discretized in time with the second-order Newmark finite difference method. We see in Figure 8 that the MHM solution is in perfect accordance with the reference solution despite the coarse non-aligned mesh being used. In addition, Figure 9 shows a zoomed-in view of the von Mises stress for both solutions in two different time steps, which illustrates how the MHM method captures the interfaces between the different layers.

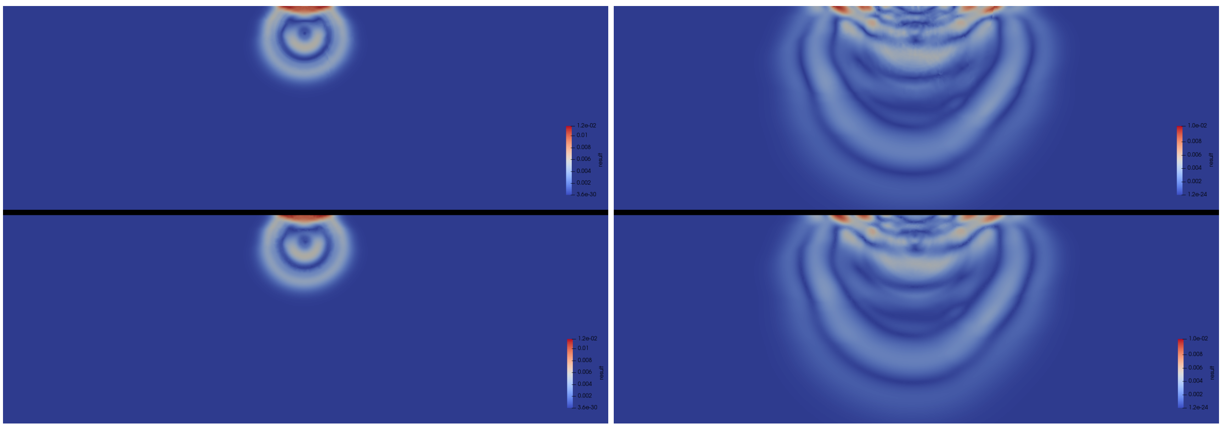

Figure 8: Isovalues of displacement magnitude for MHM (top) and the reference (bottom) at $t = 0.02$ (left) and $t = 0.11$ (right).

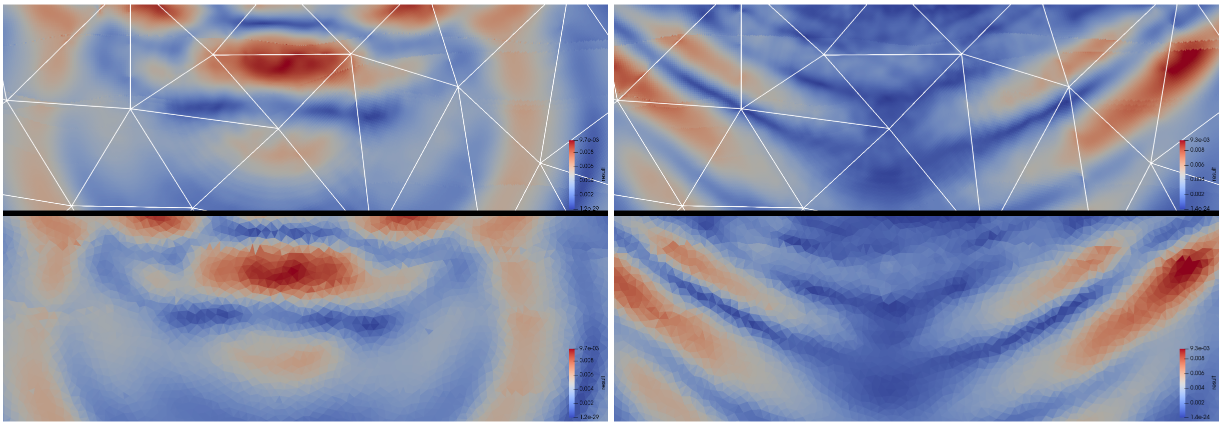

Figure 9: Isovalues of the von Mises stress for MHM with its overlying mesh (top) and the reference (bottom) at $t = 0.08$ (left) and $t = 0.15$ (right).

6 CONCLUSIONS

A new multiscale domain decomposition algorithm have been proposed for the 2D and 3D elastodynamic model with highly heterogeneous coefficients as a byproduct of the MHM methodology. The results presented herein intended to be a proof of concept of these algorithms in terms of mathematical (i.e. accuracy) terms. The numerical tests highlighted the super-convergence and the local conservative aspects of the approximate solutions (displacement, velocity and stress), and pointed out that the total discrete energy of the system is exactly preserved. These mathematical and computational performances are ready to be combined with the intrinsic flexibility of the MHM methods in incorporating local space interpolations and local time stepping driven within space and time adaptivity processes.

ACKNOWLEDGEMENTS

The authors were funded by CNPq/Brazil and CONYCIT/Chile. These research results have received funding from the EU H2020 Programme and from MCTI/RNP-Brazil under the HPC4E Project, grant agreement N 689772. The numerical results employed HPC resources from the Santos Dumont (SDumont) supercomputer at LNCC, Brazil.

REFERENCES

Abdulle, A., Weinan, E., Engquist, B., & Vanden-Eijnden, E., 2012. The heterogeneous multiscale method. *Numer. Math.*, vol. 21, pp. 1–87.

Araya, R., Harder, C., Paredes, D., & Valentin, F., 2013. Multiscale Hybrid-Mixed method. *SIAM J. Numer. Anal.*, vol. 51, n. 6, pp. 3505–3531.

Araya, R., Harder, C., Poza, A., & Valentin, F., 2017. Multiscale hybrid-mixed method for the Stokes and Brinkman equations – the method. *Comp. Meth. Appl. Mech. Eng.*, vol. 324, pp. 29–53.

Arbogast, T., 2004. Analysis of a two-scale locally conservative subgrid upscaling for elliptic problems. *SIAM J. Numer. Anal.*, vol. 42, n. 2, pp. 576–598.

Babuska, I. & Osborn, E., 1983. Generalized finite element methods: their performance and their relation to mixed methods. *SIAM J. Num. Anal.*, vol. 20, n. 3, pp. 510–536.

de la Puente, J., 2016. HPC4E Seismic Test Suite. Copyright Josep de la Puente (Barcelona Supercomputing Center) 2016. Licenced under the Creative-Commons Attribution-ShareAlike 4.0 International License.

Efendiev, Y. & Wu, X., 2002. Multiscale finite element problems with highly oscillatory coefficients. *Numer. Math.*, vol. 90, pp. 459–486.

Harder, C., Madureira, A., & Valentin, F., 2016. A hybrid-mixed method for elasticity. *ESAIM: Math. Model. Num. Anal.*, vol. 50, n. 2, pp. 311–336.

Harder, C., Paredes, D., & Valentin, F., 2013. A family of multiscale hybrid-mixed finite element methods for the Darcy equation with rough coefficients. *J. Comput. Phys.*, vol. 245, pp. 107–130.

Harder, C. & Valentin, F., 2016. *Foundations of the MHM method*, volume 114 of *Lecture Notes in Computational Science and Engineering*, chapter Building Bridges: Connections and Challenges in Modern Approaches to Numerical Partial Differential Equations, pp. 401–433. Springer.

Hesthaven, J., 2003. High-order accurate methods in time-domain computational electromagnetics. *Adv. Imag. Electr. Phys.*, vol. 127, pp. 59–123.

Hou, T. & Wu, X., 1997. A multiscale finite element method for elliptic problems in composite materials and porous media. *J. Comput. Phys.*, vol. 134, n. 1, pp. 169–189.

Lanteri, S., Paredes, D., Scheid, C., & Valentin, F., 2017. The multiscale hybrid-mixed method for the maxwell equations in heterogeneous media. HAL 01393011, INRIA.

Raviart, P. & Thomas, J., 1977. Primal hybrid finite element methods for 2nd order elliptic equations. *Math. Comp.*, vol. 31, n. 138, pp. 391–413.

Raviart, P. A., Thomas, J. M., Ciarlet, P. G., & Lions, J.-L., 1983. *Introduction à l'analyse numérique des équations aux dérivées partielles*. Masson, Paris.

Shewchuk, J. R., 1996. Triangle: Engineering a 2D quality mesh generator and Delaunay triangulator. In *Applied computational geometry towards geometric engineering*, pp. 203–222. Springer.

Si, H., 2015. TetGen, a Delaunay-based quality tetrahedral mesh generator. *ACM Transactions on Mathematical Software (TOMS)*, vol. 41, n. 2, pp. 11.